Construction and Building Materials 201 (2019) 447–460

Contents lists available at ScienceDirect

Construction and Building Materials

journal homepage: www.elsevier.com/locate/conbuildmat

Studying the fracture parameters and size effect of steel fiber-reinforced self-compacting concrete

Mohammad Ghasemi, Mohammad Reza Ghasemi, Seyed Roohollah Mousavi *

Civil Engineering Department, University of Sistan and Baluchestan, Zahedan, Iran

HIGHLIGHTS

- Fracture parameters have been calculated and compared using WFM and SEM methods.
- Steel fibers can, specifically, increase energy absorption and ductility.
- Large aggregates reduce energy absorption in self-compacting steel fiber-reinforced concrete.
- Steel fibers can perform better in lower water-cement ratios.

ARTICLE INFO

Article history:
Received 4 May 2018
Received in revised form 18 December 2018
Accepted 24 December 2018

Keywords:
Steel fiber
Fracture parameters
Size effect
Self-compacting concrete

ABSTRACT

This paper studies the laboratory results of fracture parameters and brittleness of self-compacting steel fiber-reinforced concrete. A total number of 180 different-size notched beams were built and tested under three-point bending with varying water to cement ratio, the maximum aggregate size, and different percent by volume fraction of steel fibers. To investigate and analyze the fracture parameters, use was made of SEM (Size Effect Method) and WFM (Work Fracture Method). Results have shown that in both methods, an increase in percent steel fibers increases the fracture energy and makes the concrete more ductile, but in WFM, the results are more specified because it considers the post-peak. Results show that fibers can, in some cases, reduce the size effect. The fracture energy was calculated through both WFM and SEM and the G_F/G_f was found to be about *9.66* for self-compacting steel fiber-reinforced concrete.

1. Introduction

Concrete plays an important role in the construction industry and its weakness in tension has led many researchers to study the use of steel fibers in it. Nowadays, **SFRC** is used in the construction of sidewalks, parking lots, tunnels, and bridges [1–3]. Fibers function as a bridge on both sides of a crack, absorb more concrete energy, and prevent the crack to grow. The kind, type, genus, length, strength, and distribution direction of fibers each cause different fiber behavior in concrete and, hence, different crack behavior. Fibers play important parts in the concrete technology; they increase ductility and reduce risks in concrete buildings [4,5].

The **SCC** moves, under its own weight, in the mold and between the bars without detachment and has a good performance [6]. The fiber distribution in **SCC** is a subject many researchers have commented on. Alberti et al. [7–9] have reported that although fiber positioning is affected by the concrete type, compaction method, wall effects, and so on, fibers are randomly added to the mix. Abrishambaf et al. [10] have shown that this distribution is random, but Vandewall et al. [5] believe that it is uniform (aligned); it is worth noting, however, that they have used 2 m long mother beams in their research. Some researchers have studied the effects of the volume of fibers on the mechanical properties of **SCC** and have shown that percent fiber with optimum volume can positively affect such properties and percentages higher than the optimal value would reduce the efficiency and cause segregation in **SCC** [11,12].

In recent years, many researchers have worked on the energy absorption of fibers. They prevent the crack growth in concrete and increase the energy absorption. Alberti et al. [9] have shown that adding fibers in the NVC and **SCC** will increase the energy absorption considerably, especially in the post-peak. Kazemi et al. [13] have studied the fracture energy in high-strength concrete using WFM and SEM and have shown that when steel fibers are added to concrete, the fracture energy is increased and concrete becomes more ductile. In their study, Tran et al. [14] used high-strength concrete under high strain rates, utilized smooth

* Corresponding author.
E-mail address: s.r.mousavi@eng.usb.ac.ir (S.R. Mousavi).

https://doi.org/10.1016/j.conbuildmat.2018.12.172
0950-0618/

Nomenclature

Acronyms

SCC	self compacting concrete
FRC	fiber reinforced concrete
FR-SCC	fiber reinforced self-compacting concrete
SFR-SCC	steel fiber reinforced self-compacting concrete
SF	steel fiber
SFRC	steel fiber reinforced concrete
WFM	work fracture method
SEM	size effect method
NVC	normal vibrated concrete
LEFM	line elastic fracture mechanics

Symbols

w/c	water to cement ratio
d_{max}	maximum aggregate size (mm)
V_f	fiber volume of fraction
G_F	fracture energy calculated by work fracture method (N/m)
L_{ch}	characteristic length parameter
G_f	fracture energy calculated by size effect method (N/m)
L_{ch}	characteristic length
h_{sp}	height of the remaining ligament of the beam section (mm)
f_{MOR}	flexural strength at the peak load
δ_{MOR}	deflection capacity at the peak load
f_{R2}	residual flexural strength corresponding to deflection 1.31 mm
f_{R3}	residual flexural strength corresponding to deflection 2.15 mm
f_{R4}	residual flexural strength corresponding to deflection 3 mm
$f_{R\text{-}L/150}$	residual flexural strength corresponding to deflection L/150
a_0	notch depth
N_{th}	theoretical number of fibers in the cross section [#]
N_{exp}	number of fibers counted in the cross section [#]
l_f	length of steel fiber
d_f	diameter of steel fiber
b	width of the beam section
h	height of the beam section
ρ_s	density of the steel fiber kg/m^3
G	amount of fiber in concrete kg/m^3
α	orientation factor
α_1	orientation factor in bulk [32]
α_2	orientation factor in one boundary condition [32]
α_3	orientation factor in two-boundary condition [32]
$T_{P-\delta}$	toughness calculated by the area of load deflection curve up to the point of $l/150$
$T_{f-\delta/L}$	normalized toughness calculated by the area of stress-normalized deflection curve up to the point of $l/150$

and twisted steel fibers, made notched and un-notched beams, and tested them. Their results showed that smooth fibers and notched specimens had higher fracture strength compared to twisted fibers and un-notched specimens.

A change in any concrete constituent material (maximum aggregate size, aggregate volume, cement, and w/c) or adding such materials as fly ash, Nano-silica, and fibers to concrete can affect its rheological properties, especially, its fracture behavior. Mihashi et al. [15] have shown that in NVC, the fracture energy would increase with an increase in the aggregate size. Beygi et al. [16] have reported that in **SCC**, the fracture energy would increase with an increase in the maximum aggregate size and aggregate volume. In this study, they changed the maximum aggregate size in the range 9.5–19 mm and the aggregate volume from 30 to 60%. In another study [17], they investigated the effect of w/c on the fracture energy of the **SCC** and showed that an increase in w/c reduced the fracture energy and the concrete had a more ductile behavior. Koksal et al. [18] conducted a research on the effects of w/c in steel fiber-reinforced high-strength concrete. They used varying w/c (0.35, 0.45, and 0.55) and two types of fibers with different tensile strengths (1050 and 2000 N/mm^2). Results of their research showed that in high-strength steel-fiber reinforced concrete, the fracture energy and the characteristic length parameter changed with a change in the w/c and the fiber type.

Results of researches show that adding fibers changes the concrete properties and causes its different failure behavior. Ghasemi et al. [19] showed that a change in the maximum aggregate size will cause the fracture behavior of the **SFR-SCC** to be different from that of the fiber-less one. Therefore, considering insufficient research in this regard, effort has been made in this research to add new variables and study the effects of the V_f, d_{max} and w/c on the fracture parameters of **SCC** using **SEM** and **WFM** methods. For this purpose, some notched beams were made in an experimental plan and subjected to three-point bending tests with a strain control device (Fig. 1) the results of which will be presented in the following sections.

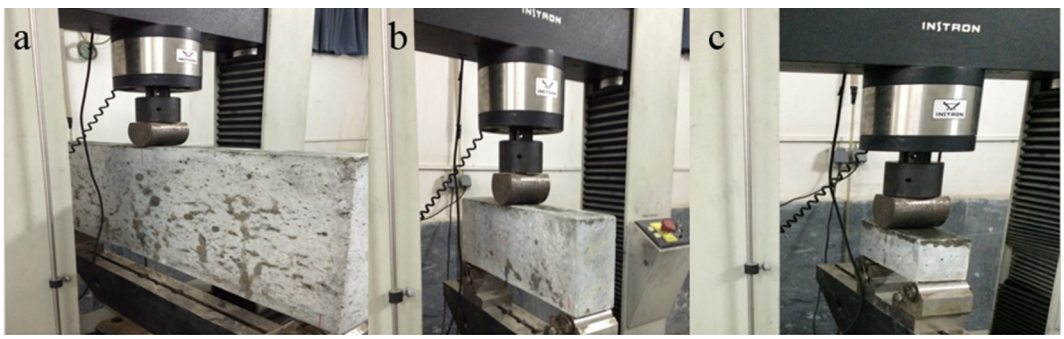

Fig. 1. Test setup of specimens with d = 400 mm (a), d = 200 mm (b), d = 100 mm (c).

Table 1
Mix proportion of concrete series and fresh properties.

Materials		Weight (kg/m^3)														
		SCCSF1	SCCSF2	SCCSF3	SCCSF4	SCCSF5	SCCSF6	SCCSF7	SCCSF8	SCCSF9	SCCSF10	SCCSF11	SCCSF12	SCCSF13	SCCSF14	SCCSF15
Cement (kg)		425	425	425	375	375	375	325	325	325	375	375	375	375	375	375
Steel fiber (kg/m^3)		23.5	23.5	23.5	23.5	23.5	23.5	23.5	23.5	23.5	39	39	39	7.8	7.8	7.8
Steel fiber (%)		0.3	0.3	0.3	0.3	0.3	0.3	0.3	0.3	0.3	0.5	0.5	0.5	0.1	0.1	0.1
Sand (kg)		846	846	846	846	846	846	846	846	846	846	846	846	846	846	846
Coarse aggregate	4.75–9.5 (mm)	750	300	300	750	300	300	750	300	300	750	300	300	750	300	300
	9.5–12.5 (mm)	–	450	300	–	450	300	–	450	300	–	450	300	–	450	300
	12.5–19 (mm)	–	–	150	–	–	150	–	–	150	–	–	150	–	–	150
Limestone powder		180	180	180	180	180	180	180	180	180	180	180	180	180	180	180
Free water (kg)		178	178	178	195	195	195	201	201	201	195	195	195	195	195	195
Superplasticizer (kg)		5.3	5.3	5.3	3.75	3.75	3.75	3	3	3	4.5	4.5	4.5	3	3	3
Unit weight (kg/m^3)		2238	2245	2290	2200	2260	2320	2280	2345	2385	2257	2295	2360	2340	2320	2400
Flow time (s)		3.2	2.9	3	3	2.6	2.98	2.5	2.2	2.4	3.01	2.88	3.45	2.98	2.80	2.85
Slump flow (mm)		700	710	740	590	715	655	690	700	700	630	670	690	600	650	670
L-Box (h_2/h_1)		0.95	0.94	0.95	0.82	0.88	0.83	0.89	0.86	0.9	0.81	0.85	0.89	0.83	0.86	0.9
Sieve test (%)		1	1.8	1	1	2.9	1	1.2	2	1.6	1.2	1	1.2	1	1	1.3
W/C (by weight)		0.42	0.42	0.42	0.52	0.52	0.52	0.62	0.62	0.62	0.52	0.52	0.52	0.52	0.52	0.52

2. Experimental work

2.1. Mix design

To study the fracture parameters of the **SFR-SCC**, 15 lab designs, including 180 different-size notched beams, were prepared wherein the d_{max} = 9.5, 12.5, and 19 mm to study the effects of the maximum aggregate size on the fracture parameters. To study the effects of water to cement ratio on fracture parameters, $\boldsymbol{w/c}$ = 0.42, 0.52, and 0.62 were considered. Moreover, to assess the effects of steel fibers on fracture parameters, $\boldsymbol{V_f}$ = 0.1, 0.3, and 0.5% were considered so that the fresh concrete could pass the conditions in EFNARC [20]. A list of concrete constituents/specifications is given in Table 1.

2.2. Materials

Materials used in this lab design include type II Portland cement (with physical and chemical properties listed in Table 2), ultrafine

Table 2
Portland cement type II chemical and physical properties.

Chemical analysis		Results
Sio_2 (%)		21.05
Al_2O_3 (%)		4.76
Fe_2O_3 (%)		3.43
CaO (%)		62.86
Mgo		3.46
SO_3		1.87
Na_2O (%)		0.21
K_2O (%)		0.58
CL		0.04
$LO.I$ (%)		1.2
$I.R$ (%)		0.53
C_3S (%)		53.4
C_2S (%)		20.1
C_3A (%)		6.9
C_4AF (%)		10.4
$F.CaO$ (%)		3.2
Physical test		
$Blanic$ (cm^2/kg)		3110
$SettingTime$ (min)	$Initial$	183
	$Final$	238
$Autoclave.\ Exp$ (%)		0.08

Fig. 2. Steel fiber employed in this study.

Table 3
Determination of beam specimen in SEM.

Aggregate size (mm)	Steel fiber Length (mm)	d (mm)	b (mm)	a_0/d	S/d	L/d
9.5, 12.5, 19	30	100 200 400	100	0.2	2.5	2.67

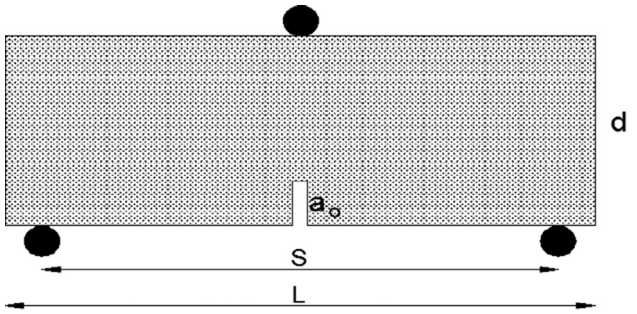

Fig. 3. Geometry of the three-point bending specimen.

limestone powder to increase viscosity, fine aggregates consisting of natural sand with a fineness modulus of 2.8, coarse aggregates made of natural crushed gravel with maximum size of 9.5, 12.5, and 19 mm and specific gravity of 2.93 g/cm^3, super viscose with modified carboxylate base (according to SIA 162 AND PREN 934-2 Standard for concrete with steel fibers) so that the **SFR-SCC** can have the required performance (according to EFNARC [20]), and hooked steel fibers (Fig. 2) with a tensile strength of 1200 N/mm^2 and a diameter of 0.6 mm. The fiber length was 30 mm constant for all the specimens.

2.3. Test method

Laboratory tests were done on fracture parameters of **SFR-SCC** to determine the relationship between the effects of the maximum aggregate size, water to cement ratio and the volume fraction of steel fibers. Fracture parameters were calculated by **WFM** according to RILEM 50 FMC [21] and mold sizes were selected according to ASTM 1609 [22] which requires the mold width (b) should be at least 3 times the fiber length (it was taken equal to 100 mm for all specimens). Three $350 \times 100 \times 100$ mm (length, height, width) notched beam specimens were made and tested for each design; the notch height in all designs was 0.33 d (ASTM 1609). In **SEM**, the specimens were made according to RILEM TC 89 [23] which requires the beam width (b) should be at least 3 times the maximum aggregate size, but ASTM 1609 requires it to be at least 3 times the fiber length; here, it was taken equal to 100 mm for all specimens. Other beam dimensions (a_0/d, S/d, and L/d) are respectively 0.2, 2.5, and 2.67 based on the RILEM TC 89 (Table 3 & Fig. 3).

The notch width, created by an acrylic sheet, is 0.3 mm in both methods. Six 150×300 mm standard cylinders were made to calculate the compressive strength, Splitting tensile strength, and modulus of elasticity based on BSEN 12390 [25], ASTM C 469 [26], and ASTM C496 [27]. Fresh concrete tests (Slump Flow, Flow

Table 4
Value of G_F measured from beam tested in mixtures by WFM.

MIX ID	Steel fiber (Vf) (%)	f_c (MPa)	E (GPa)	f_t (MPa)	Average G_F	Average L_{ch}
SCCSF1	0.3	23	25	2.7	425.41	1514
SCCSF2	0.3	21.5	26.3	2.6	517.16	1921
SCCSF3	0.3	30.53	30.2	3.2	701.24	2025
SCCSF4	0.3	26.15	23	4.17	367.9	485.7
SCCSF5	0.3	27.55	24.48	3.58	483	922.55
SCCSF6	0.3	27.41	27.13	3.85	463	844.51
SCCSF7	0.3	21	20.2	2.26	189.25	741.06
SCCSF8	0.3	20.5	22	1.8	254.97	1604.12
SCCSF9	0.3	23	24	2.3	384.87	1746.13
SCCSF10	0.5	23.75	20.19	3.22	480.48	935.63
SCCSF11	0.5	22.25	23.91	2.93	647	1793.8
SCCSF12	0.5	30.15	30.62	3.12	491	1395.11
SCCSF13	0.1	32.4	27.54	3.55	226.19	492.53
SCCSF14	0.1	24.55	26.95	3.13	317.51	873
SCCSF15	0.1	25.49	28.05	3.28	249.25	647.35

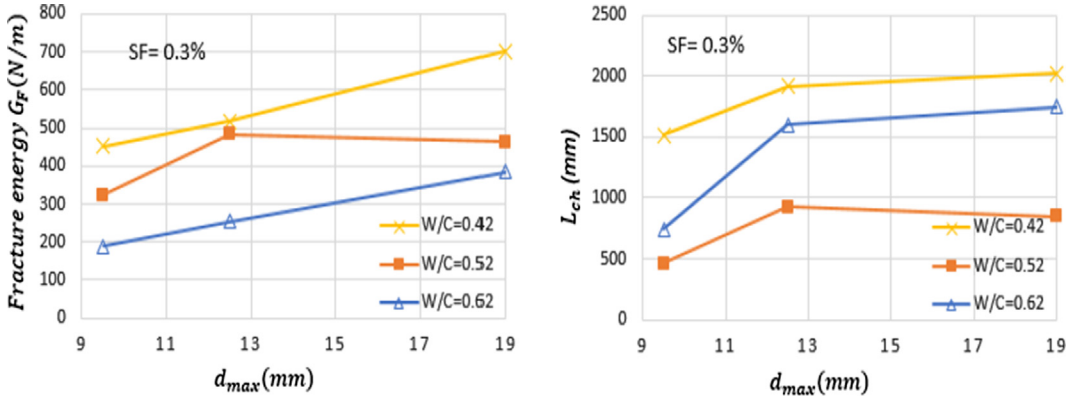

Fig. 4. Variation of the total fracture energy with maximum size of coarse aggregate (Left), Variation of the L_{ch} with maximum size of coarse aggregate (Right).

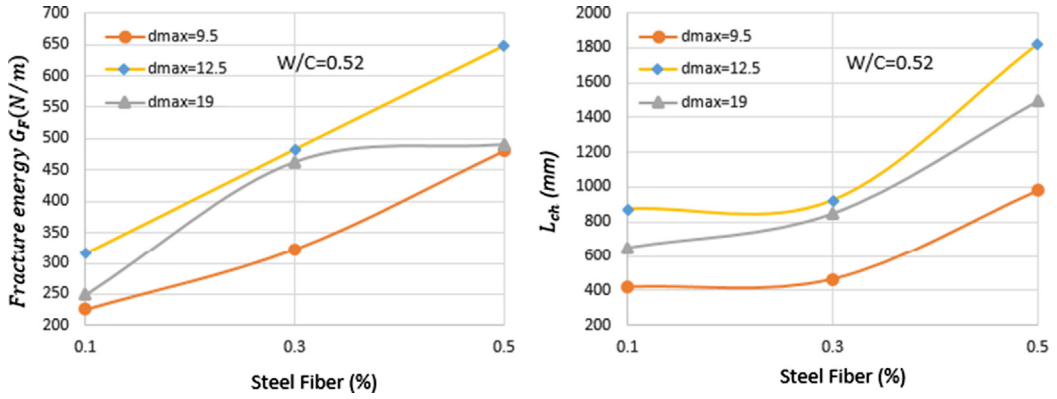

Fig. 5. Variation of the total fracture energy with volume fraction of steel fiber (Left), Variation of the L_{ch} with volume fraction of steel fiber (Right).

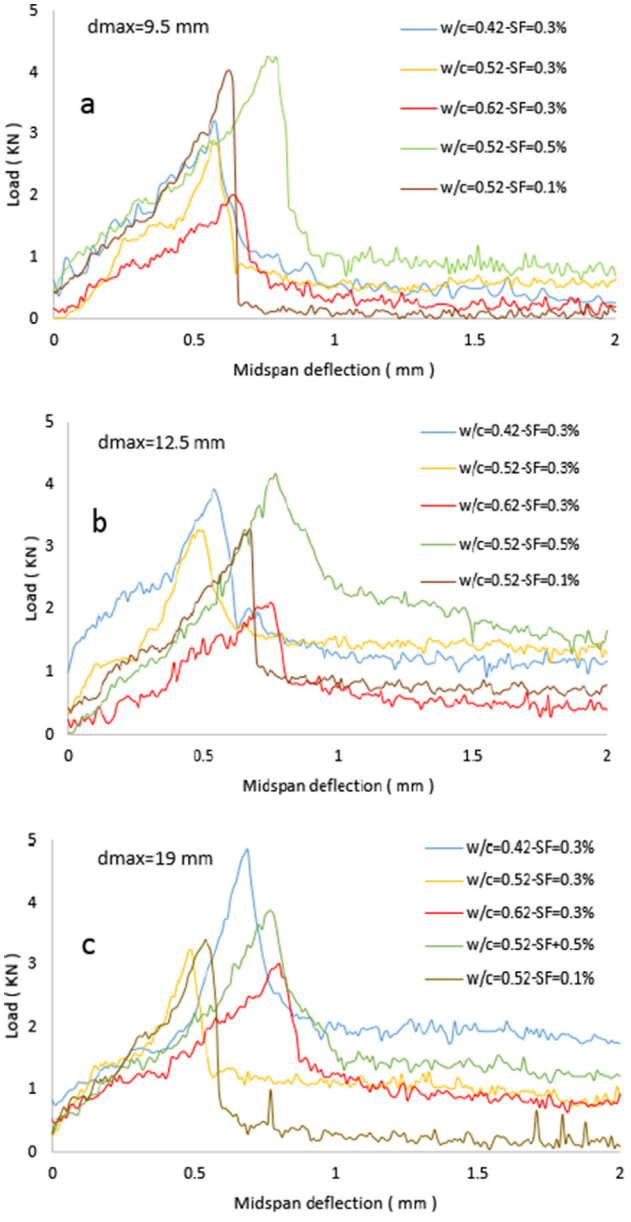

Fig. 6. Load–midspan deflection curves obtained for all mixes by WFM (a: *dmax* = 9.5, b: *dmax* = 12.5, c: *dmax* = 19 mm).

Time, L-Box, and Sieve test) were carried out based on EFNARC [20] requirements. After being made, the specimens were kept in the lab for 24 h and then immersed in a water tank for 28 days at 20 ± 2 °C untill the test day.

RILEM TC 162 [28] and BS EN 14651 [29] explicitly state that concrete pouring should begin at the center of the mold. Some researchers [30] believe that in steel fiber-reinforced self-compacting concrete, pouring from one end of the mold is preferable. Alberti et al. [31] have shown that in self-compacting concrete, pouring at the center can reduce fiber dispersion. In this study, since we used different-size molds to evaluate the size effect, and it was not possible to start pouring at one end of the smallest mold, we did at the center and continued the process similarly for all specimens for uniform results.

3. Calculating fracture parameters

3.1. WFm

There are several methods for calculating fracture parameters among which WFM (recommended in RILEM 50 FMC [21]) is very simple and widely used by many researchers. First proposed by Hillerborg [24], WFM is based on the 3-point bending test of notched beams under strain control test and its fracture energy is found as follows:

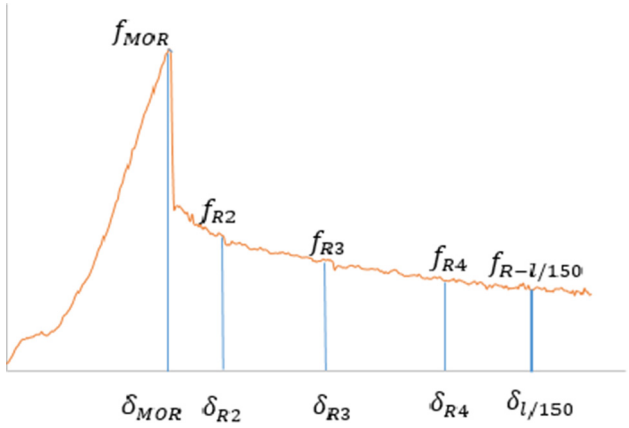

Fig. 7. Load deflection diagram and f_R.

$$G_F = \frac{W_F}{b(d-a_0)} \quad (1)$$

where W_F is the area under the load-displacement curve, b is the specimen width, d is the specimen height, and a_0 is the notch depth. Since Hillerborg believed that G_F alone could not show the concrete brittleness or ductility, he introduced the characteristic length parameter as follows:

$$L_{ch} = \frac{EG_F}{f_t^2} \quad (2)$$

where E is the elastic modulus and f_t is the tensile strength; lower L_{ch} values represent more brittle behavior of concrete.

3.2. SEm

Using small lab specimens for the behavior modeling of large structures is an issue that shows the importance of size effect for which a method was first presented by Bazant and Peiffer [33]. In this method, also suggested in RILEM TC 89, a three-point bending test is used to calculate the fracture parameters of different-size notched beams and the nominal strength of similar-geometry specimens can be explained by its rule as follows:

$$\sigma_N = \frac{B}{\sqrt{1+\beta}}, \ \beta = \frac{d}{d_0} \quad (3)$$

Table 5
Residual strength of concrete from WFM.

MIX ID	δ_{MOR} (mm)	f_{MOR} (MPa)	f_{R2} (MPa)	f_{R3} (MPa)
SCCSF1	0.58	3.141848	0.54	0.2552
SCCSF 2	0.54	3.829127	1.2525	1.1561
SCCSF 3	0.69	4.712772	1.8654	1.70481
SCCSF 4	0.57	2.8473	0.4698	0.6381
SCCSF 5	0.49	3.190939	1.3663	1.2763
SCCSF 6	0.48	3.141848	1.2362	0.8627
SCCSF 7	0.65	1.963655	0.1928	0.1816
SCCSF 8	0.75	2.061838	0.3829	0.3709
SCCSF 9	0.81	2.758935	0.3745	0.371
SCCSF 10	0.76	4.123675	0.8568	0.6872
SCCSF 11	0.77	4.025493	2.0863	1.6445
SCCSF 12	0.77	3.789854	1.41026	1.1781
SCCSF 13	0.62	3.92731	0.1472	0.1227
SCCSF 14	0.67	3.240031	0.7854	0.7854
SCCSF 15	0.54	3.240031	0.2552	0.0981

Table 6
Comparison of the experimental and theoretical number of fibers.

Mix ID	G (kg/m^3)	α	N_{th} Calc (#)	N_{exp} Exp (#)	Ratio *calc*/*exp*
SCCSF1	23.55	0.519	37	27	1.37
SCCSF 2	23.55	0.519	37	31	1.19
SCCSF 3	23.55	0.519	37	34	1.08
SCCSF 4	23.55	0.519	37	24	1.54
SCCSF 5	23.55	0.519	37	31	1.19
SCCSF 6	23.55	0.519	37	27	1.37
SCCSF 7	23.55	0.519	37	20	1.85
SCCSF 8	23.55	0.519	37	21	1.76
SCCSF 9	23.55	0.519	37	26	1.42
SCCSF 10	39.25	0.519	61	31	1.96
SCCSF 11	39.25	0.519	61	45	1.35
SCCSF 12	39.25	0.519	61	40	1.52
SCCSF 13	7.85	0.519	12	9	1.33
SCCSF 14	7.85	0.519	12	10	1.20
SCCSF 15	7.85	0.519	12	9	1.33
Average of all beams					1.43
Coefficient of variation					17.8%

Table 7
Corrected maximum loads from SEM for mixes.

MIX ID	$\acute{f}_c$ (MPa)	a_0/d	Depth d (mm)	Corrected maximum load P_0(N)		
				Beam 1	Beam 2	Beam 3
SCCSF1	23	0.2	100	6955.5	7155.5	6755.5
			200	12,422	12,222	12,722
			400	20,888	21,888	22,388
SCCSF2	21.5	0.2	100	7555	7055	6755
			200	11,220	11,420	10,720
			400	18,680	18,880	19,380
SCCSF3	30.53	0.2	100	9555.75	9055.75	10065.75
			200	17,323	16,383	15,433
			400	27,892	25,792	26,092
SCCSF4	26.15	0.2	100	6855	7365	6655
			200	10,900	12,500	14,455
			400	19,280	20,380	19,980
SCCSF5	27.55	0.2	100	7056.5	7396.5	7356.5
			200	12,226	14,226	12,426
			400	18,104	21,104	21,704
SCCSF6	27.41	0.2	100	6858	7734	7258
			200	12,232	12,492	12,737
			400	19,328	18,928	18,828
SCCSF7	21	0.2	100	5056	5156	5856
			200	7624	8424	9224
			400	13,896	14,896	15,296
SCCSF8	20.5	0.2	100	5855	5255	5455
			200	8220	8420	8120
			400	13,880	13,580	14,880
SCCSF9	23	0.2	100	6156.22	5856.22	5656.22
			200	9524.9	10324.9	9724.9
			400	17899.6	17599.6	16999.6

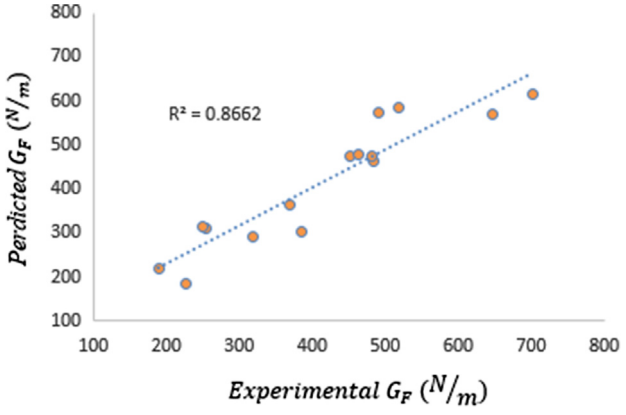

Fig. 8. Experimental result versus predicted value from the proposed relation for G_F.

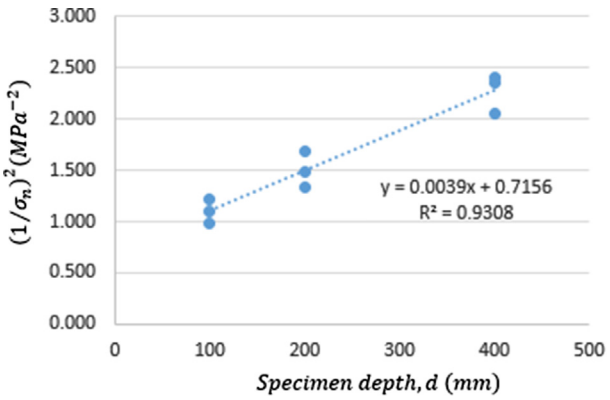

Fig. 9. Linear regression for size effect parameters.

where β is the ductility number first presented by Bazant and kazemi [34]. When $\beta < 0.1$, the concrete behavior resembles that of the limit state, when $\beta > 10$, it is close to linear fracture mechanism, and when $0.1 < \beta < 10$, it is nonlinear. B and d_0 are experimental coefficients that depend on the material property, specimen geometry, and maximum load; for different-size specimens, they are found as follows using regression analysis:

$$Y = AX + C,\ X = d,\ Y = \left(\frac{1}{\sigma_N}\right)^2,\ d_0 = \frac{C}{A},\ B = \frac{1}{\sqrt{C}} \tag{4}$$

Bazant & Kazemi also showed that G_f and C_f can be calculated as follows:

$$G_f = \frac{g(\alpha_0)}{AE} \tag{5}$$

$$C_f = \frac{g(\alpha_0)}{\acute{g}(\alpha_0)} \times \frac{C}{A} \tag{6}$$

where E is the elastic modulus, A is the slope of the regression line, C is the Y-intercept of the regression line, $g(\alpha_0)$ is the dimensionless

Table 8
Fracture parameters obtained from the SEM for mixes.

Series	f_c (MPa)	E (GPa)	a_0/d	$g(\alpha_0)$	G_f(N/m)	C_f (mm)	B (MPa)	d_0 (mm)	K_{IC} (MPa mm$^{0.5}$)	δ_c (mm)	ω_A	ω_c	m
SCCSF1	23	25	0.2	7.28	66.47	72	0.77	378.93	40.76	0.044	0.06	0.04	0.04
SCCSF2	21.45	26.3	0.2	7.28	35.11	33.34	0.85	175.27	30.38	0.021	0.14	0.23	0.16
SCCSF3	30.53	30.2	0.2	7.28	61.96	34.97	1.182	183.81	43.25	0.027	0.1	0.15	0.11
SCCSF4	26.15	23	0.2	7.28	47.34	38.60	0.858	202.92	33.01	0.028	0.19	0.26	0.2
SCCSF5	27.55	24.48	0.2	7.28	42.55	30.55	0.943	160.62	32.27	0.023	0.11	0.2	0.14
SCCSF6	27.41	27.13	0.2	7.28	31.48	21.69	1.014	114.012	29.22	0.016	0.05	0.12	0.07
SCCSF7	21	20	0.2	7.28	29.36	41.06	0.611	215.83	24.23	0.024	0.19	0.24	0.19
SCCSF8	20.5	22	0.2	7.28	21.79	27.58	0.673	145	21.89	0.016	0.17	0.32	0.21
SCCSF9	23	24	0.2	7.28	40.642	59.67	0.653	313.64	32.23	0.032	0.16	0.14	0.13
SCCSF10	23.75	20.19	0.2	7.28	53.57	38.51	0.857	202.44	32.94	0.0323	0.13	0.18	0.14
SCCSF11	22.25	23.91	0.2	7.28	48.54	36.37	0.912	191.18	34.07	0.027	0.16	0.24	0.18
SCCSF12	30.11	30.62	0.2	7.28	47.69	27.67	1.174	145.46	38.21	0.020	0.1	0.19	0.12
SCCSF13	32.4	27.54	0.2	7.28	45.06	30.29	1.03	159.23	35.23	0.022	0.08	0.15	0.1
SCCSF14	24.55	26.95	0.2	7.28	39.47	33.83	0.906	177.83	32.61	0.022	0.17	0.27	0.2
SCCSF15	25.49	28.05	0.2	7.28	49.14	49.25	0.855	258.87	37.13	0.029	0.21	0.22	0.19

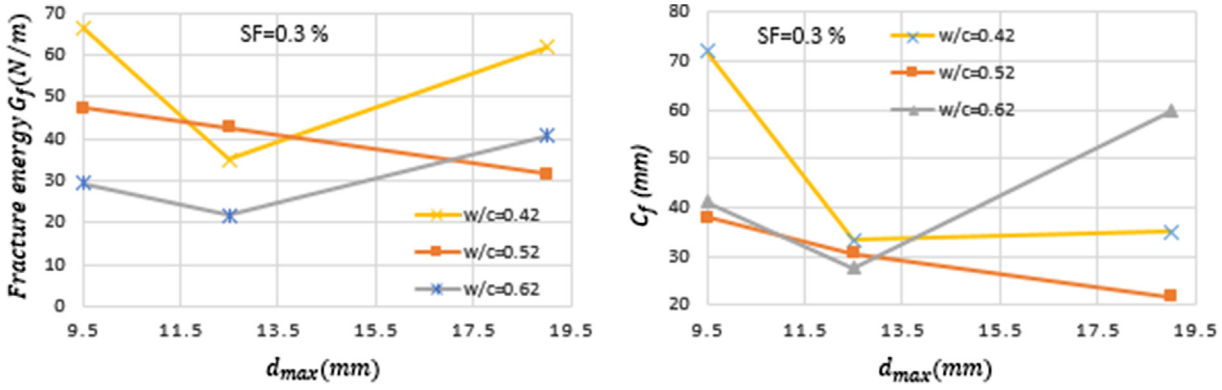

Fig. 10. Variation of the G_f (Left) and C_f (Right) from size effect method with maximum size of coarse aggregate for mixes.

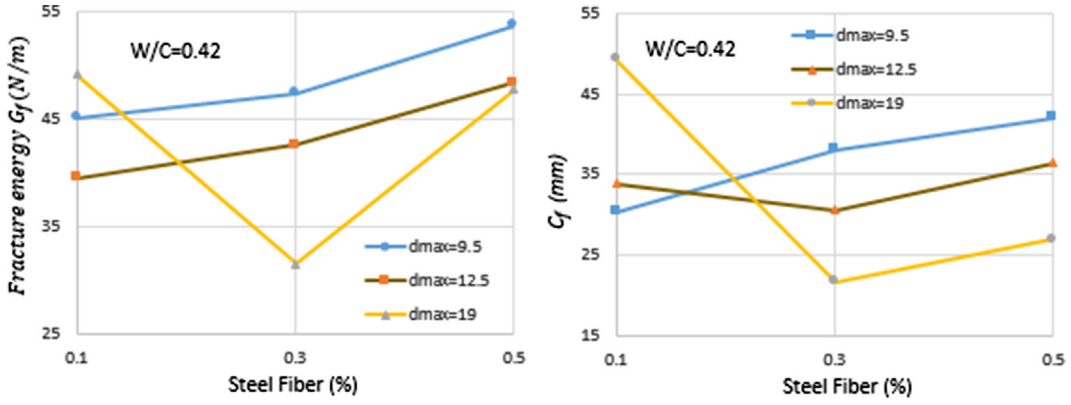

Fig. 11. Variation of the G_f (Left) and C_f (Right) from size effect method with volume fraction of steel fiber.

parameter of the energy dissipation rate, and $\acute{g}(\alpha_0)$ is the derivative of $g(\alpha_0)$ where $(\alpha_0 = \frac{a_0}{d})$. Eq. $g(\alpha_0)$ and $\acute{g}(\alpha_0)$ are geometry dependent and are determined according to LEFM. In SEM, such parameters as fracture toughness (K_{IC}) and effective crack tip opening displacements are found as follows:

$$K_{IC} = \sqrt{EG_f} \tag{7}$$

$$\delta_C = \frac{8K_{IC}}{E}\sqrt{\frac{C_f}{2\pi}} \tag{8}$$

4. Results analysis

4.1. WFm

As mentioned earlier, the fracture energy (G_F) is found through the area under the load-displacement curve (up to $l/150$) and characteristic length parameter (L_{ch}) based on Eq. (2) recommended in RILEM 50 FMC [21] and the results are shown in Table 4 and Figs. 4 and 5; Fig. 4 shows the fracture energy variations versus d_{max} with different w/c (in these mix designs, $V_f = 0.3\%$ fix). Earlier, researchers had reported that when w/c increases, G_F is reduced and L_{ch} is increased, and when d_{max} increases, both G_F and L_{ch} increase too [16,17]. Results of this study show that when w/c increases, the fracture energy decreases, but at $w/c = 0.42$, L_{ch} shows different behavior maybe because a reduced w/c reduces the porosity. This porosity reduction around fibers increases the fiber-concrete bonding strength resulting fibers to resist being pulled out of the concrete and, hence, perform better in the post-peak.

Results of Fig. 4 also show that when the maximum aggregate size increases, G_F increases too, but L_{ch} increases at maximum aggregate sizes from 9.5 to 12.5, and at size 19, the increase is little or there is even a decrease because at this size, fibers have less space to move (or rotate) and tend more to lie obliquely or even vertically (parallel to the fracture surface). The best fiber positioning at the fracture surface is horizontal (perpendicular to the fracture surface). In these cases, the fiber efficiency is reduced in the post-peak and fibers may act as voids and cause crack growth and reduce energy absorption. Fig. 5 shows fracture energy variations versus percent fiber variations at different maximum aggregate sizes. Here, $w/c = 0.52$. When $d_{max} = 9.5$ and 12.5 mm, an increase in percent fiber increases the fracture energy and concrete exhibits a more ductile behavior. When $d_{max} = 19$ mm and $V_f = 0.5\%$, the fracture energy growth is negligible because, as mentioned earlier, at this size the fibers have less space for movement and an increase in percent fiber will disturb the fracture matrix; microcracks grow and energy absorption is reduced.

Fig. 6 shows the mid-span load-deflection curve for all specimens. RILEM TC 162 [28] and BS EN 14651 [29] suggest the use of the following equation to calculate the residual flexural tensile strength (f_R) for different FRC deflections:

$$f_R = \frac{3F_l L}{2bh_{sp}^2} \tag{9}$$

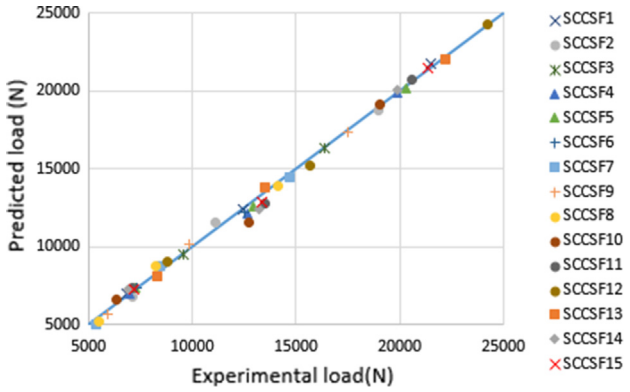

Fig. 13. Experimental and predicted peak load.

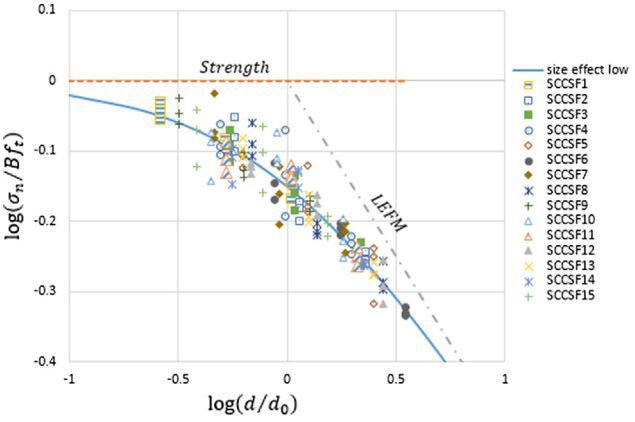

Fig. 14. Size effect plot of **SCCSF** specimens with various of w/c, $dmax$ and v_f.

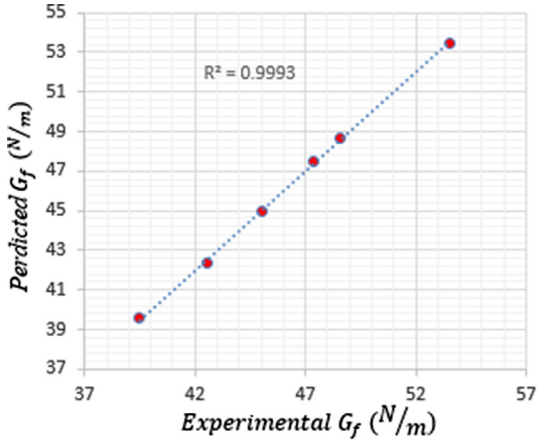

Fig. 12. Experimental result versus predicted value from the proposed relation for G_f.

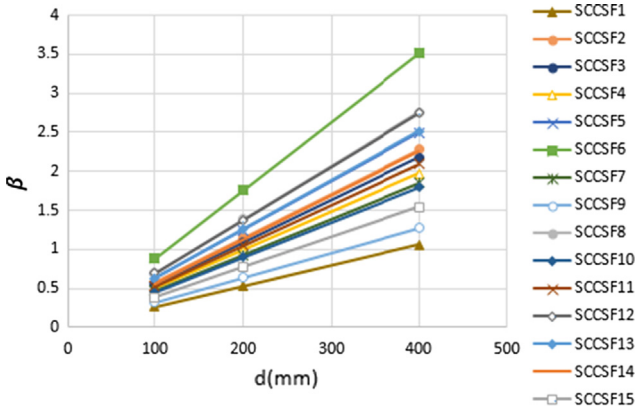

Fig. 15. Variation of brittleness number with depth.

The limit of proportionally (*LOP*) is taken as the highest load in the deflection interval of 0.0 mm to 0.05 mm. But, our findings show that f_{LOP} in the load-deflection curve is very small (also reported in the work of other researchers e.g. [10,13,35,36]). Hence, in this study, only f_{MOR}, f_{R2} and f_{R3} have been found at δ_{MOR}, $\delta = 1.31$ and $\delta = 2.15$, respectively (Fig. 7 & Table 5). According to Table 5, at $w/c = 0.62$ and $V_f = 0.1$ the residual strength is the lowest, and according to Fig. 6, at $w/c = 0.52$, the concrete behavior, especially at post-peak, is sometimes close to $w/c = 0.42$ and sometimes close to $w/c = 0.62$ due, perhaps, to close w/c values selected. But, the concrete behavior at post-peak for w/c values of 0.42–0.62 shows that an increase in the w/c will cause a decrease in the residual strength. Fig. 6 also shows the effects of the increased fibers on the post-peak.

Another point worth discussing about the **FRC** is the fiber distribution at the fracture surface. Many researchers [7,8,32] have worked on the calculation of the fibers at the fracture surface. Dupton and Vandewall [32] have suggested the following equation for this purpose:

$$N_{th} = \frac{G \times \alpha}{\frac{\pi \times d_F^2}{4} \times \rho_s} \times b \times h_{sp} \tag{10}$$

The orientation factor (α) is calculated using the following equation:

$$\alpha = \frac{\alpha_1 (b - l_f)(h - l_f - a_0) + \alpha_2 \left[(b - l_f) \frac{l_f}{2} + \left(h - \frac{l_f}{2} - a_0 \right) l_f \right] + \alpha_3 \frac{l_f^2}{2}}{b(h - a_0)} \tag{11}$$

where α_1 is the orientation factor in bulk (here,$\alpha_1 = 0.5$), α_2 is the orientation factor of a fiber with 1 boundary condition (here,α_2

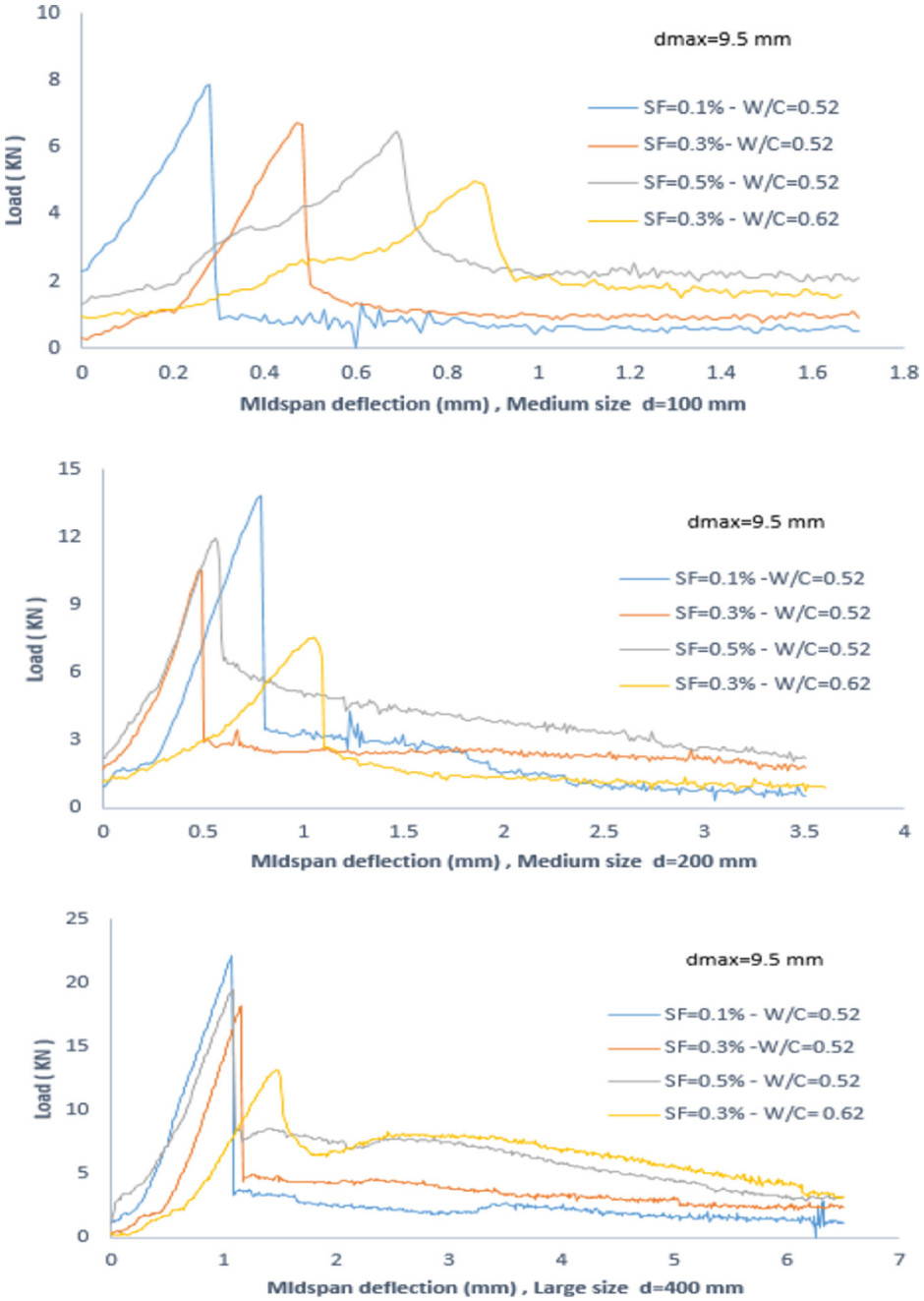

Fig. 16. Load–midspan deflection curves obtained for $d_{max} = 9.5$ mm by SEM(d = 100, 200 and 400 mm).

= 0.6), α_3 is the orientation factor of a fiber with 2 boundary conditions (here,α_3 = 0.84) (Table 6). As shown, predicting the fiber distribution pattern at the fracture surface is a difficult task because several factors (mixing, pouring, mold size, concrete type, fiber type, fiber material, etc.) can affect this distribution.

Using all the experimental results and doing regression analyses on all the data, a relationship has been proposed (in this study) as follows that depends on the maximum aggregate size, water to cement ratio and percent by volume of steel fibers:

$$G_F = -206.09 - 3.307d_{max}^2 - 1692.975\left(\frac{w}{c}\right)^2 - 833.420V_f^2 + 209.25d_{max}\left(\frac{w}{c}\right) + 404.462d_{max}V_f + 2504.779\left(\frac{w}{c}\right)V_f - 793.88\left(\frac{w}{c}\right)d_{max}V_f \quad (12)$$

Eq. (12) is used to predict the fracture energy and Fig. 8 shows that it can predict experimental results with good approximation.

4.2. SEm

In SEM, only peak load will suffice to calculate the fracture parameters and post-peak is not required; peak load results from testing all mix designs are listed in Table 7. After calculating the peak load, it is necessary to use a regression analysis for each mix design; for mix design No. 3, for instance, the regression line is shown in Fig. 9. As shown, the slope and intercept found from regression are A = 0.0039 and C = 0.715; in addition, variation coefficient of slope (w_A), variation coefficient of intercept (w_c), and relative width of scatter band (m) are respectively 0.1, 0.15, and 0.11. According to RILEM TC 89 [23], w_A should not be greater than 0.1

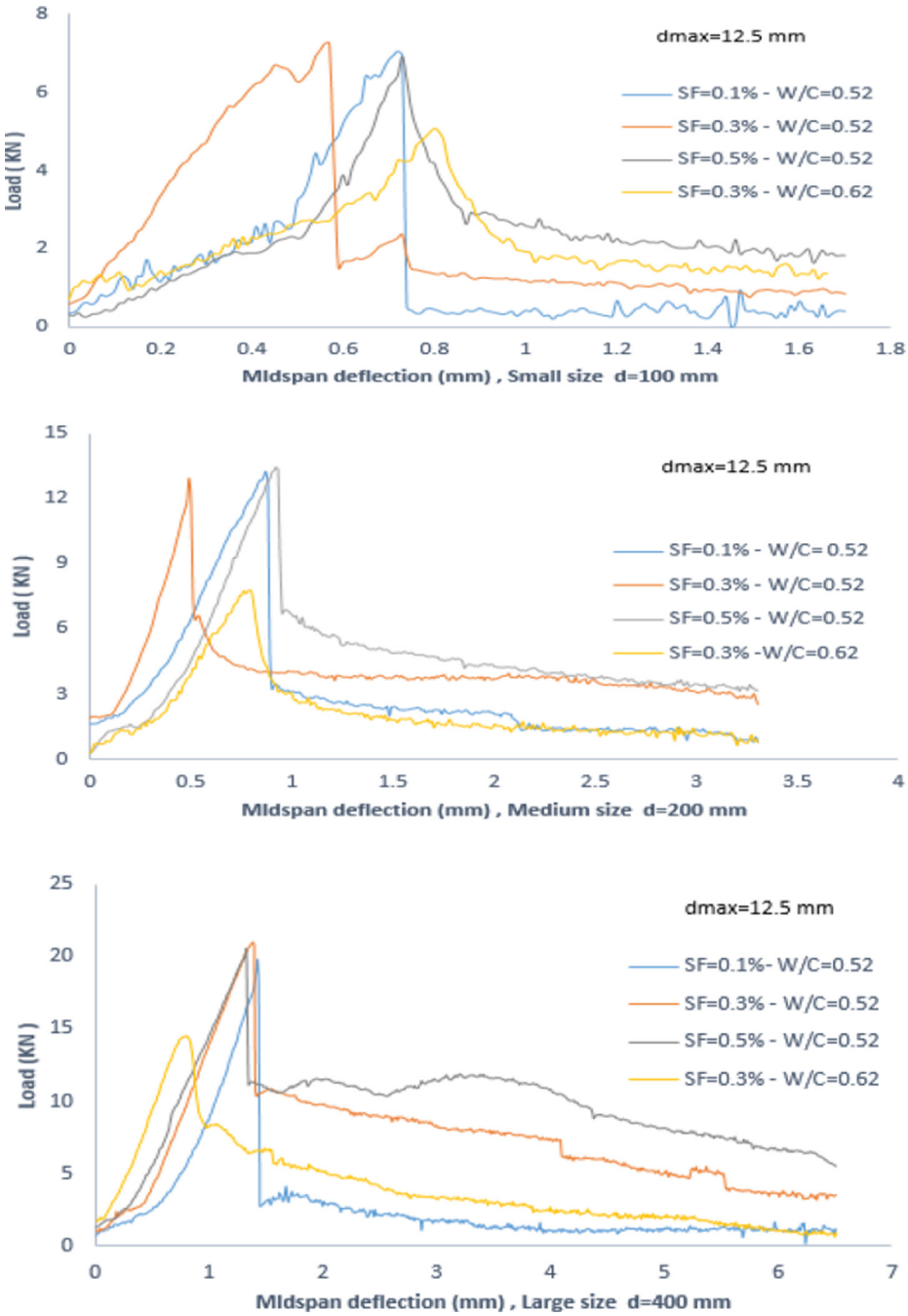

Fig. 17. Load–midspan deflection curves obtained for d_{max} = 12.5 mm by SEM(d = 100,2 00 and 400 mm).

and w_c and m should not exceed 0.2. As shown in Table 8, there is difference in some mix designs; some researchers have reported that sometimes fibers cause a drop in the compressive strength [12], and have reasoned that since fibers are distributed randomly, some of them lie parallel to the load direction and act like a void causing the growth of micro-cracks and reduced strength. In SEM, since only peak load is effective and post-peak is not calculated, sometimes fibers cause dispersion in peak load results. Fig. 10 shows G_f and C_f variations versus the largest aggregate size for varying w/c. As shown, there is confusion in the peak load results because, as mentioned earlier, fibers are present in the fracture matrix and create confusion in it. Larger size aggregates too can intensify this phenomenon because they limit the fiber movement (or rotation) space [37]. But, ignoring the results from d_{max} = 19 mm at w/c = 0.42 and 0.62, it can be generally concluded that when the largest aggregate size is increased, the fracture energy is decreased and the concrete becomes more ductile. It can also be concluded that the fiber orientation in the fracture surface is directly related to the peak load. Fig. 11 shows the results from the fracture energy versus percent fiber for different values of d_{max}. As shown, when percent fiber increases, G_f increases too and the concrete becomes more ductile. Similarly, when the largest

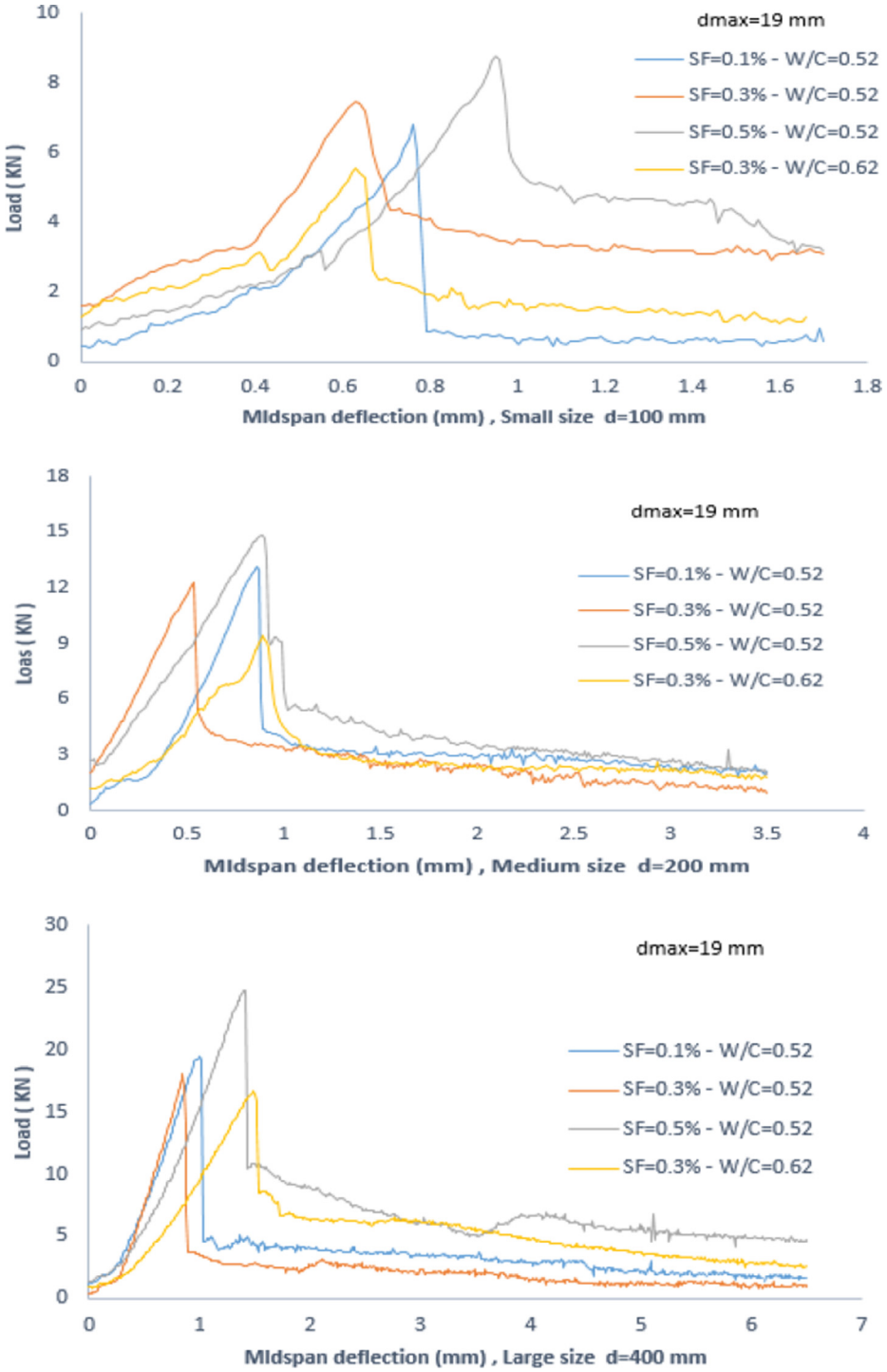

Fig. 18. Load–midspan deflection curves obtained for d_{max} = 19 mm by SEM(d = 100,200 and 400 mm).

aggregate size is increased, the fracture energy is reduced and the concrete shows a more brittle behavior. Different behavior of d_{max} = 19 mm at V_f = 0.1% can be attributed to the fact that since percent fiber is low, the concrete behavior is closer to that of fiber less concrete and an increase in the largest aggregate size increases the fracture energy. Kazemi et al. [13] showed that there is a linear relationship between the fracture energy and the percent by volume of fibers; the present study too shows similar result in d_{max} = 9.5 and 12.5 mm (Fig. 11):

$$d_{max} = 9.5\text{mm} : G_f = 21.27V_f + 42.274, R^2 = 0.93 \quad (13)$$

$$d_{max} = 12.5\text{mm} : G_f = 22.67V_f + 36.718. R^2 = 0.96 \quad (14)$$

Koksal et al. [18] used two variables V_f and w/c and showed that the fracture energy can be calculated using a polynomial function. In the present research, a relationship, that depends on V_f and d_{max}, has been presented as follows using nonlinear regression analyses on the results.

$$G_f = 128.183 + 0.552d_{max}^2 + 42.87V_f^2 + 0.467d_{max}V_f - 14d_{max} - 8.88V_f \quad (15)$$

Fig. 12 shows that Eq. (15) can acceptably predict the lab results. Fig. 13 shows that the results from lab tests and from the SEM prediction conform well. Fig. 14 shows the SEM curve fitted by the experimental data from 15 mix designs; as shown, there is a good overlap between the results from empirical data and those from the SEM. Bazant's size effect law shows that the closer are the results to the strength criterion, the more ductile will the concrete behave, and the closer are the results to the line elastic fracture mechanic (LEFM) criteria, the more brittle will the concrete behave. Another important parameter in SEM is the brittleness coefficient (β) which is most often used to calculate the fracture mode. Results of Fig. 15 show that for all mix designs with varying d_{max}, β lies within the range of the nonlinear fracture mechanics ($0.1 \leq \beta < 10$).

Figs. 16–18 show the SEM load-deflection curves for all specimens. As mentioned in Section 4.1, f_{LOP} is small at a deflection of 0.05 mm. Table 9 shows the residual strength for different deflections. Results show that specifically at d_{max} = 12.5 mm, an increase in percent fiber, increases the post peak residual strength for different-size specimens. According to ASTM 1609, deflection for all specimens has been measured up to $l/150$ only, and $T_{P-\delta}$ (area under the load deflection curve) too, has been calculated up to this same point (Fig. 7). To be able to study the effects of the residual strength for different-size specimens, their sizes should be normalized [38,39]; therefore, the deflection is divided by the specimen's span length to calculate the normal deflection. $T_{f-\delta/L}$ is the area under the normalized stress-deflection curve the results of which are shown in Table 9. Fig. 19 shows the size effect on the normal-

Table 9
Summary of average parameters characterizing the flexural performance and size effect.

Mix ID	Size	f_{MOR}(MPa)	δ_{MOR} (mm)	δ/l (%)	$T_{p-\delta}$ (kN mm)	f_{R2} (MPa)	f_{R3} (MPa)	f_{R4} (MPa)	$f_{R-l/150}$ (MPa)	$T_{f-\delta/l}$ (Pa)
4	Small	3.93	0.47	0.18	2.52	0.49	0	0	0.58	5.91
	Medium	3.1	0.48	0.1	9.44	0.73	0.72	0.67	0.54	5.29
	Large	2.66	1.15	0.11	25.76	0.7	0.64	0.58	0.36	3.81
5	Small	4.25	0.57	0.2	3.87	0.62	0	0	0.5	9.08
	Medium	3.79	0.49	0.1	13.44	1.13	1.12	0.9	0.74	7.87
	Large	3.06	1.31	0.138	47.65	2.95	1.37	1.19	0.51	6.98
6	Small	4.48	0.64	0.25	6.04	1.85	0	0	1.86	14.17
	Medium	3.59	0.53	0.1	10.51	0.88	0.57	0.41	0.39	6.16
	Large	2.48	0.85	0.08	16.72	0.4	0.42	0.34	0.15	2.45
7	Small	2.91	0.86	0.34	3.56	0.87	0	0	0.93	8.35
	Medium	2.13	1.06	0.21	7.7	0.56	0.375	0.32	0.3	4.22
	Large	1.9	1.45	0.14	39.47	1.67	1.02	1.18	0.47	5.78
8	Small	2.97	0.8	0.32	3.58	0.92	0	0	0.76	8.4
	Medium	2.27	0.79	0.15	7.12	0.62	0.41	0.33	0.23	4.17
	Large	2.12	0.8	0.08	26.36	0.99	0.7	0.47	0.14	3.86
9	Small	4.45	0.63	0.25	3.51	1.85	0	0	1.86	14.17
	Medium	2.47	0.92	0.18	10.23	0.82	0.7	0.67	0.54	5.99
	Large	2.44	1.49	0.14	35.099	2.08	0.93	0.91	0.38	5.14
10	Small	3.79	0.69	0.27	4.67	1.31	0	0	1.28	10.95
	Medium	3.49	0.56	0.11	14.68	1.34	1.09	0.79	0.71	8.6
	Large	2.62	1	0.1	42.09	1.21	1.03	1.09	0.47	6.16
11	Small	4.05	0.73	0.29	4.05	1.25	0	0	1.07	9.5
	Medium	3.91	0.92	0.18	15.44	1.57	1.19	1.02	0.94	9.04
	Large	2.93	1.31	0.13	62.1	2.93	1.64	1.67	0.81	9.1
12	Small	5.12	0.95	0.38	6.46	2.75	0	0	1.96	15.14
	Medium	4.38	0.89	0.17	16.71	1.39	0.97	0.77	0.96	9.79
	Large	3.68	1.41	0.14	47.64	3.37	1.21	0.9	0.67	6.97
13	Small	4.61	0.28	0.11	2.37	0.36	0	0	0.37	5.56
	Medium	4.05	0.79	0.15	9.61	0.85	0.44	0.25	0.14	5.63
	Large	3.24	1.07	0.1	22.19	0.52	0.38	0.28	0.17	3.25
14	Small	4.13	0.72	0.2	2.45	0.38	0	0	0.23	5.7
	Medium	3.81	0.86	0.17	10.21	0.72	0.41	0.41	0.24	5.98
	Large	2.64	1.43	0.14	17.94	2.35	0.34	0.25	0.16	2.62
15	Small	3.66	0.76	0.3	2.48	0.44	0	0	0.45	5.18
	Medium	3.85	0.86	0.17	11.73	0.96	0.81	0.68	0.66	6.87
	Large	2.85	1	0.1	25.85	0.65	0.58	0.51	0.23	3.74

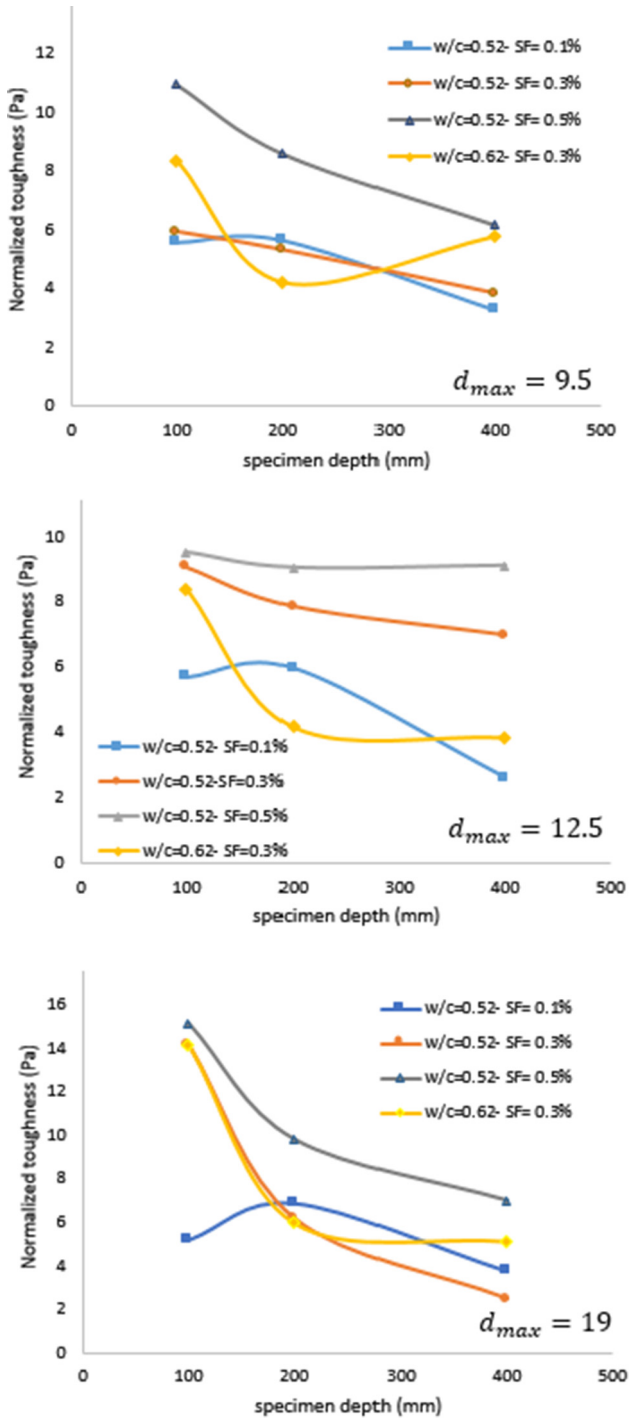

Fig. 19. Size effect on normalized toughness at $l/150$ ($dmax$ = 9.5, 12.5 and 19 mm).

ized toughness; the highest value of the size effect can be observed at d_{max} = 19 mm and the lowest is at d_{max} = 12.5 mm. Results also show that an increase in w/c does not specifically influence the size effect.

Since post-peak is calculated in WFM, G_F is always larger than G_f. Bazant and Becq-giradun [40] showed G_F/G_f = 2.5 in **NVC** and Beygi et al.[14] showed G_F/G_f = 3.11 in **SCC**. Kazemi et al. [13] have shown that in high strength steel fiber-reinforced concrete, G_F/G_f is about 10.5. In this study, G_F/G_f values for 15 mix designs are listed in Table 10; the average value is 9.66 with a variation coefficient of 32%.

Table 10
Relationship between WFM and SEM.

MIX ID	Steel fiber (vf) (%)	dmax	G_F/G_f
SCCSF1	0.3	9.5	6.7
SCCSF2	0.3	12.5	14.7
SCCSF3	0.3	19	11.32
SCCSF4	0.3	9.5	7.77
SCCSF5	0.3	12.5	11.35
SCCSF6	0.3	19	14.7
SCCSF7	0.3	9.5	6.44
SCCSF8	0.3	12.5	11.69
SCCSF9	0.3	19	9.47
SCCSF10	0.5	9.5	8.93
SCCSF11	0.5	12.5	13.32
SCCSF12	0.5	19	10.29
SCCSF13	0.1	9.5	5.01
SCCSF14	0.1	12.5	8.04
SCCSF15	0.1	19	5.07
Average			9.66
variation coefficient			32%

5. Conclusions

In this study, the effects of w/c, the maximum aggregate size, and percent by volume of fibers on the fracture parameters of the **SFR-SCC** have been investigated by constructing different-size notched beams according to the RILEM recommendation. Results show that a change in each parameter will cause a change in the energy absorption and fracture parameters; this is quite clear in the results.

- In WFM, an increase in w/c decreases the fracture energy and concrete becomes more ductile, but in lower w/c, since fibers perform better in post-peak, concrete ductility is increased. Results of this method have shown that when maximum aggregates size are used in concrete, energy absorption is decreased because fibers have less space for rotation. Results have also shown that when percent fiber is increased, the fracture energy Increases and concrete becomes more ductile; d_{max} = 12.5 is the most suitable aggregate for **SFR-SCC** because it has shown the best results.
- In SEM, use is only made of the initial part of the load-displacement curve up to the peak load; post-peak is not used. The main fiber performance in concrete is in the post-peak; it increases the energy absorption. Results show that in the **SFR-SCC**, when the maximum aggregate size increases, it causes a disruption in the fracture matrix and confusion in the results. Presence of fibers in the fracture matrix and their lying in the load direction can cause a drop in the peak load; however, with this method too, it can be concluded that an increase in the percent fiber increases the fracture energy and the concrete becomes more ductile.
- -Since fibers show their effects in the post-peak, it can be concluded that WFM yields better results than SEM in **SFR-SCC**.
- Results show that: 1) size effect does exist in **SFR-SCC**, but at d_{max} = 12.5 mm, an increase in percent fiber can reduce it and 2) w/c does not particularly affect the size effect.
- Results show that predicting the fiber distribution pattern at the fracture surface is a difficult task because several factors (concrete mixing/pouring/flow/type, fiber type/material, mold size, etc.) can affect this distribution.

Conflict of interest

No potential conflict of interest.

References

[1] L. Sorelli, A. Meda, G.A. Plizzari, Steel fiber concrete slabs on ground: a structural matter, ACI Struct. J. 103 (4) (2006) 551–558.
[2] A. Fuente, P. Pujadas, A. Blanco, A. Aguado, Experiences in Barcelona with the use of fibres in segmental linings, Tunnel. Underground Space Technol. 27 (2012) 60–71.
[3] P. Serna, S. Arango, T. Ribeiro, A.M. Nunez, E. Garcia-Taengua, Structural cast-inplace SFRC: technology, control criteria and recent applications in Spain, Mater. Struct. 42 (9) (2009) 1233–1246.
[4] R. Zerbino, J.M. Tobes, M.E. Bossio, G. Giaccio, On the orientation of fibres in structural members fabricated with self-compacting fibre reinforced concrete, Cem. Concr. Compos. 34 (2) (2012) 191.
[5] L. Vandewalle, G. Heirman, F. Van-Rickstal, Fiber orientation in self-compacting fibre reinforced concrete, Proc. of the 7th Int. RILEM Symp on Fibre Reinforced Concrete: Des and Appl, 2008.
[6] H. Okamura, M. Ouchi, Self-compacting concrete, J. Adv. Concr. Technol. 1 (2003) 5–15.
[7] M.G. Alberti, A. Enfedaque, J.C. Gálvez, On the prediction of the orientation factor and fibre distribution of steel and macro-synthetic fibres for fibre-reinforced concrete, Cem. Concr. Compos. (2017) 29–48.
[8] M.G. Alberti, A. Enfedaque, J.C. Gálvez, A review on the assessment and prediction of the orientation and distribution of fibres for concrete, Compos. B: Eng. 151 (2018) 274–290.
[9] M.G. Alberti, A. Enfedaque, J.C. Galvez, Comparison between polyolefin fibre reinforced vibrated conventional concrete and self-compacting concrete, Constr. Build. Mater. 85 (2015) 182–194.
[10] A. Abrishambaf, V. Cunha, J. Barros, A two-phase material approach to model steel fibre reinforced self-compacting concrete in panels, Eng. Fract. Mech. 162 (2016) 1–20.
[11] M. Beygi, J. Berenjian, O. Omran, A.S. Nik, I.M. Nikbin, An experimental survey on combined effects of fibers and nano-silica on the mechanical, rheological, and durability properties of self-compacting concrete, Mater. Des. 50 (2013) 1019–1029.
[12] R. Madandoust, M.M. Ranjbar, R. Ghavidel, F. Shahabi, Assessment of factors influencing mechanical properties of steel fiber reinforced self-compacting concrete, Mater. Des. 83 (2015) 284–294.
[13] M.T. Kazemi, H. Golsorkhtabar, M.H.A. Beygi, M. Gholamitabar, Fracture properties of steel fiber reinforced high strength concrete using work of fracture and size effect methods, Constr. Build. Mater. 142 (2017) 482–489.
[14] N.T. Tran, T.K. Tran, J.K. Jeon, J.K. Park, D.J. Kim, Fracture energy of ultra-high-performance fiber-reinforced concrete at high strain rates, Cem. Concr. Res. 1 (2015) 169–184.
[15] H. Mihashi, N. Nomura, S. Niiseki, Influence of aggregate size on fracture process zone of concrete detected with 3D acoustic emission technique, Cem. Concr. Res. 21 (1991) 737–744.
[16] M.H.A. Beygi, M.T. Kazemi, I.M. Nikbin, J.V. Amiri, S. Rabbanifar, E. Rahmani, The influence of coarse aggregate size and volume on the fracture behavior and brittleness of self-compacting concrete, Cem. Concr. Res. 66 (2014) 75–90.
[17] M.H.A. Beygi, M.T. Kazemi, I.M. Nikbin, J.V. Amiri, The effect of water to cement ratio on fracture parameters and brittleness of self-compacting concrete, Mater. Des. 50 (2013) 267–276.
[18] F. Koksal, Y. Sahin, O. Gencel, I. Yigit, Fracthure energy-based optimization of steel fiber reinforced concretes, Eng. Fract. Mech. 107 (2013) 29–37.
[19] M. Ghasemi, M.R. Ghasemi, S.R. Mousavi, Investigating the effects of maximum aggregate size on self-compacting steel fiber reinforced concrete fracture parameters, Constr. Build. Mater. 162 (2018) 674–682.
[20] EFNARC, The European Guidelines for Self-Compacting Concrete, Specification, Production and Use, 2005.
[21] RILEM FMC-50, Determination of the fracture energy of mortar and concrete by means of three-point bending tests on notched beams, Mater. Struct. 18 (4) (1985) 287–290.
[22] ASTM C 1609/C 1690M-07, in: Standard Test Method for Flexural Performance of Fiber Reinforced Concrete (Using Beam with Third-point Loading), 2007, pp. 1–8.
[23] RILEM FMT-89, Size-effect method for determining fracture energy and process zone size of concrete, Mater. Struct. 23 (6) (1990) 461–465.
[24] A. Hillerborg, Results of three comparative test series for determining the fracture energy GF of concrete, Mater. Struct. 18 (1985) 407–413.
[25] BS EN 12390, Part 3: Testing Hardened Concrete. Method of determination of Compressive Strength of Concrete Cubes, British Standards Institution, 2000.
[26] ASTM C 469, Standard Test Method for Static Modulus of Elasticity and Poisson's Ratio of Concrete in Compression, American Society of Testing and Materials, 2004.
[27] ASTM C 496, Standard Test Method for Splitting Tensile Strength of Cylindrical Concrete Specimens, American Standards for Testing and Materials, 2011.
[28] RILEM TC 162-TDF, Test and design methods for steel fibre reinforced concrete: bending test (final recommendation), Mater. Struct. 35 (2002) 579–582.
[29] BS EN 14651:2007+A1, Test Method for Metallic Fibre Concrete. Measuring the Flexural Tensile Strength (Limit of Proportionality (LOP), Residual), 2007.
[30] S. Grünewald, Performance-based Design of Self-compacting Fibre Reinforced concrete, Delft University Press, Delft (The Netherlands), 2004.
[31] M.G. Alberti, A. Enfedaque, J.C. Gálvez, Fracture mechanics of polyolefin fibre reinforced concrete: study of the influence of the concrete properties, casting procedures, the fibre length and specimen size, Eng. Fract. Mech. 154 (2016) 225–244.
[32] L. Dupont, L. Vandewalle, Distribution of steel fibres in rectangular sections, Cem. Concr. Compos. 27 (3) (2005) 391–398.
[33] Z.P. Bazant, P. Pfeiffer, Determination of fracture energy from size effect and brittleness number, ACI Mater. J. 84 (6) (1987) 463–480.
[34] Z.P. Bazant, M.T. Kazemi, Determination of fracture energy, process zone length and brittleness number from size effect, with application to rock and concrete, IJFr 44 (1990) 111–131.
[35] A. Noushini, M. Hastings, A. Castel, F. Aslani, Mechanical and flexural performance of synthetic fibre reinforced geopolymer concrete, Constr. Build. Mater. 186 (2018) 454–475.
[36] M. Ahmadi, S. Farzin, A. Hassani, M. Motamedi, Mechanical properties of the concrete containing recycled fibers and aggregates, Constr. Build. Mater. 144 (2017) 392–398.
[37] L. Jiaping, L. Changfeng, L. Jiangzhong, D. Zhaojing, C. Gong, Characterization of fiber distribution in steel fiber reinforced cementations composites with low water-binder ratio, Indian J. Eng. Mater. Sci. 18 (2011) 449–457.
[38] D.Y. Yoo, N. Banthia, J.M. Yang, Y.S. Yoon, Size effect in normal and high-strength amorphous metallic and steel fiber reinforced concrete beams, Constr. Build. Mater. 121 (2016) 676–685.
[39] D.L. Nguyen, D.J. Kim, G.S. Ryu, K.T. Koh, Size effect on flexural behavior of ultra high performance hybrid fiber reinforced concrete, Compos. B: Eng. 45 (2013) 1104–1116.
[40] Z.P. Bazant, E. Becq-Giraudon, Statistical prediction of fracture parameters of concrete and implications for choice of testing standard, Cem. Concr. Res. 32 (4) (2002) 529–556.